Punching Shear Behavior of Externally Prestressed Concrete Slabs

H. Mostafaei[1]; F. J. Vecchio[2]; P. Gauvreau[3]; and M. Semelawy[4]

Abstract: The use of externally post-tensioned fiber-reinforced concrete decks in highway bridge structures is seen as a viable option in the move toward the design and construction of high-performance structures. However, with the thin unreinforced deck slabs that may result, punching shear is a potential concern. An experimental program is described in which the punching shear behavior of externally prestressed slabs is investigated, both with plain and fiber-reinforced concrete specimens. Results indicate that significant improvements in strength, ductility, energy absorption and nonbrittleness of failure can be achieved with fiber reinforcement. Nonlinear finite-element analysis procedures are used to model the specimens, and reasonably accurate simulations of behavior are obtained. Design code procedures are found to be unconservative in estimating the punching shear strength of these elements, whereas a commonly used analytical model is found to be overly conservative.

Introduction

Although high-performance concrete has been used extensively in bridges in Canada and the United States since the mid 1990s, its application has been motivated primarily by concerns over durability. Consequently, the high compressive strength available has remained underutilized in bridges. An efficient use of the strength of high-performance concrete requires moving toward thinner cross section components. In many cases, a significant impediment to doing this is the presence of reinforcing steel, which imposes dimensional requirements related to clear cover and spacing between bars. The deck slabs of many box girder bridges, however, are prestressed in two horizontal directions; reinforcing steel is provided primarily for crack control. In such cases, it is possible to consider replacing the reinforcing steel by steel fibers, which would create opportunities for reducing the thickness of these components.

Punching shear is an important failure mode of bridge deck slabs. The contribution of an active, known precompression force (as opposed to a passive compressive force created by restraint) and of the presence of steel fibers to the punching resistance of thin slabs is not well understood. This paper presents the results of an experimental and analytical study undertaken to characterize the effect of these two factors on the punching shear behavior of thin concrete slabs.

Previous Studies

Since the late 1950s, numerous experimental investigations have been undertaken to study the behavior of laterally-restrained slabs which, relative to unrestrained slabs, typically exhibited a large increase in load-carrying capacity. Wood (1961), for example, reported strengths greater than 10 times those predicted by yield-line theory. Taylor and Hayes (1965) identified the effects of lateral edge restraint on the punching shear strength of slabs, and concluded that code requirements for punching shear needed to be revised to take the restraint effect into consideration. Aoki and Seki (1974) studied shear behavior in the vicinity of concentrated punching loads; special attention was given to "arching action," the mechanism which explains the tendency of restrained slabs to fail in punching rather than in flexure.

Mufti et al. (1993) investigated the possibility of producing a concrete deck slab that is entirely steel-free and capable of matching the load levels resisted by conventionally-reinforced decks. Hassan et al. (2002) also studied the effect of prestressing on the punching strength of steel-free deck slabs. A system of external unbonded prestressing bars was used as the lateral confinement system, rather than the steel straps used by Mufti et al. (1993). The positive effects of prestressing were also previously reported by He (1992), who tested a $\frac{1}{4}$-scale slab-on-girder bridge segment. In many applications, the inclusion of steel fibers in concrete has proven to be beneficial to the over-all mechanical behavior of the structure. Fiber reinforced concrete (FRC) shows an improvement in toughness, ductility, energy absorption, cracking resistance, and tensile strength (Shaaban and Gesund 1994). In traditionally-

[1]Research Officer, National Research Council Canada, Institute for Research in Construction, M-59, Ottawa, ON K1A 0R6.

[2]Professor, Dept. of Civil Engineering, Univ. of Toronto, Toronto, Canada, M5S 1A4.

[3]Associate Professor, Dept. of Civil Engineering, Univ. of Toronto, Toronto, Canada, M5S 1A4.

[4]Ph.D. Candidate, Dept. of Civil Engineering, Univ. of Western Ontario, London, Canada, N6A 5B9.

reinforced slab-column connections, with and without shear reinforcement, Swamy and Ali (1982) found that fiber reinforcement changed the shape of the punching failure surface and that the ensuing failure was more gradual and ductile.

The various approaches developed to predict the ultimate punching shear strength of concrete slabs can be divided into two categories: empirical equations, based on statistical analysis of tests results; and rational mechanistic models. The mechanistic approach idealizes the failure mechanism, system geometry, and material properties to build a mathematical model that seeks to predict the punching shear strength. Hewitt and Batchelor (1975) proposed such a model to predict the behavior of restrained circular slabs that fail in punching, based on an extrapolation of the work by Kinnunen and Nylander (1960). The model was further developed by Newhook (1997) for application to laterally restrained deck slabs of slab-on-girder bridges.

Little has been reported on the punching shear behavior of externally prestressed FRC slabs, either from an analytical or experimental perspective.

Experimental Program

An experimental program was undertaken comprising seven square externally-prestressed slab specimens. Four were constructed using steel fiber reinforced concrete (SFRC); the remaining three, serving as control specimens, were constructed of plain concrete. None contained conventional internal reinforcement, and all were externally post-tensioned in two directions.

Details of the test specimens are provided in Fig. 1. The nominal dimensions of the slab and loading plate were $1500 \times 1500 \times 127$ mm and $200 \times 200 \times 50$ mm, respectively. To minimize the effect of local stress concentrations at the points of application of the post-tensioning forces, sixteen C130×10 channels, each 204 mm in length, were cast integrally along the specimen edges as shown.

The specimens were externally post-tensioned using eight 32-mm diameter Dywidag bars in each direction. The force in each Dywidag bar was transmitted first to a vertical steel beam comprised of two C310×45 channels, and then to the specimen through a $204 \times 170 \times 38$ mm plate bearing against a 32-mm-diameter round bar welded to the C130×10 channels. (For specimen P-1, the loading plates acted directly against the specimen.) The post-tensioning system details are shown in Fig. 1. The points of application of axial load were chosen to facilitate the post-tensioning process and to create a condition as close as possible to a uniform axial stress state without interfering with the applied vertical load. Linear elastic finite-element (FE) analysis indicated that a near uniform compressive stress was achieved across the widths of the specimens at the center.

The slabs rested on continuous roller supports all around, giving simple-spans of 1,350 mm in each direction. The transverse loading system for the specimens consisted of a vertical monotonically-increasing concentric load applied to a 200 mm-square steel loading plate. The load was supplied by a 5,300 kN capacity testing machine in displacement-control mode.

Linear variable differential transducers (LVDTs) were used to monitor the vertical and horizontal displacements of the specimen. The vertical displacement was measured using six to eight LVDTs; four were placed at the corners, mounted on the top surface of the slab and aligned with the centerline of the rollers, and two (four for F-1, F-3, F-4 and P-2a) were attached on opposite sides of the Baldwin machine head. The top and bottom horizon-

tal LVDTs were used to monitor axial displacements and rotations of the edges; these were placed at the midspan of each side, 9 mm away from top and bottom surfaces. Two electrical resistance strain gauges, with 5 mm gauge lengths, were applied to each Dywidag bar to measure the bar strains during post-tensioning and testing. These strains were used to monitor bar forces during the experiments. In addition, loads cells were employed at the anchored ends of two of the Dywidag bars to corroborate forces determined from the strain gauge readings.

The concrete used to construct each test specimen was custom-batched with a targeted 28-day compressive strength of 50–60 MPa. Mix proportions are given in Table 1. To maintain an adequate workability for the FRC mix, the gravel/cement ratio was reduced, and the super plasticizer content was increased. Higher cement content was needed to reach the intended concrete strength. The actual concrete compressive strengths, as determined on test days using standard cylinder tests, are reported in Table 2. Also given are the fracture energies for those specimens constructed from SFRC. [Note: The fracture energies were determined using notched prisms ($150 \times 150 \times 530$ mm) tested under 4-point bending according to the Italian Standard UNI-11039].

Dramix RC-80/50-BP steel fiber was used in the amount of 1.0% by volume, for SFRC specimens F-1, F-2, and F-3. For Specimen F-4, the same steel fiber type was used in the amount of 1.5% by volume. This high-carbon wire fiber with hooked ends has a nominal length (L) of 50 mm and a nominal diameter (d) of 0.60 mm. The tensile strength was 2000 MPa, according to manufacturer specifications.

A primary test objective was to investigate the influence of steel fibers in enhancing the punching shear capacity of the slabs. In addition, the influence from the amount and pattern of prestressing used was also to be studied. The nominal prestressing forces initially applied to the specimens are given in Table 3.

In practice, for shear punching of the bridge slabs due to the heavy trucks, the load distribution under the rubber tires could create curved boundaries. However, in this study, for the sake of simplicity and comparison, as with the previous similar tests, a square loading plate was used in the test setups. Further studies are recommended to evaluate the potential influence of the loading conditions on the slab shear punching behavior.

Test Results

All specimens failed in a punching shear mode, except Specimen P-3 which failed in a punching-flexural mode. The measured load-deflection responses are given in Fig. 2. The maximum load capacity, energy dissipation, and postpeak ductility and failure mode for each specimen are reported in Table 4.

Specimens P-1 and P-2a failed in a highly brittle punching mode. In each case, the punching failure was attained when a cone of concrete completely detached from the underside of the slab [e.g., see Fig. 3(a)] with no visible or audible warning. The suddenness of the failure was reflected in the load-deformation responses recorded [see Fig. 2(a)]. With these specimens, the shear fracture on the compressed surface of the specimen occurred immediately adjacent to the loading plate. On the tension side, cracking was aligned with the inner face of the plate, with some irregularities at the corners. The average angle of inclination of the shear failure plane, measured from the horizontal, was 15° for Specimen P-1 and 12° for Specimen P-2a. The failure mode of Specimen P-3 was interpreted as a combined flexural-punching shear failure in which both flexural cracks (i.e., cracks underneath
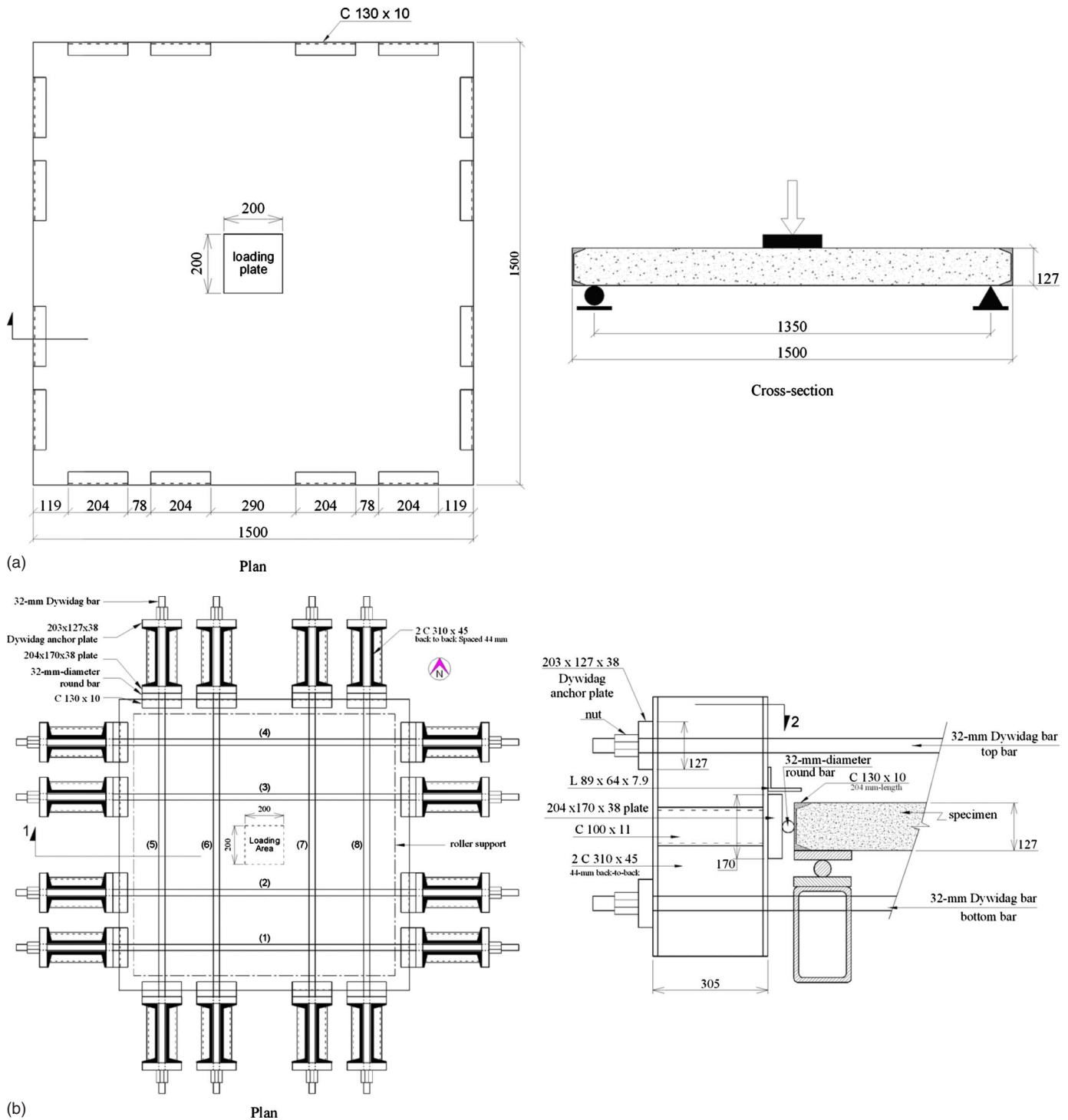
Fig. 1. Details of test specimens and post-tensioning system: (a) specimen details; (b) post-tensioning system

the slab extending from the corners to the center) and punching shear cracks (i.e., cracks from near the edge of the loading plate on the top diagonally extending to the underside of the slab) were observed to form simultaneously at failure. On the compression surface, several longitudinal flexural cracks formed approximately at midspan, while punching shear cracks formed immediately adjacent to the loading plate.

All SFRC specimens (F-1, F-2, F-3, and F-4) failed by punching shear. The failures were characterized by cracks forming around the loading plate periphery followed by penetration of the loading plate. On the tension surface, no distinguishable shear

fracture cone was evident although some longitudinal and diagonal cracks were observed [see Fig. 3(b)]. Audible signs of distress heard during the loading process were attributed to the fibers debonding and pulling out across the widening cracks. The formation of a complete failure surface for Specimens F-1, F-2, and F-3 was gradual and occurred over a few minutes resulting in a moderately ductile failure. Specimen F-4 experienced a more brittle load-deformation response with a sudden drop in load capacity occurring just after the peak, as seen in Fig. 2(b). Considering the high prestress to which it was subjected, the more brittle response of Specimen F-4 might be due to its relatively lower

Table 1. Concrete Mix Design

	Mixture	Mixture proportion	Dry weight (kg/m^3)
Plain concrete specimens	Standard type 10 Portland cement	1.00	375
	Sand	2.26	847
	Gravel (10 mm crushed limestone)	2.88	1080
	Water	0.37	139
SFRC specimens	Portland silica fume cement	1.00	450
	Sand	2.26	1018
	Gravel (10 mm crushed limestone)	1.67	750
	Water	0.39	176

Table 2. Average Concrete Properties

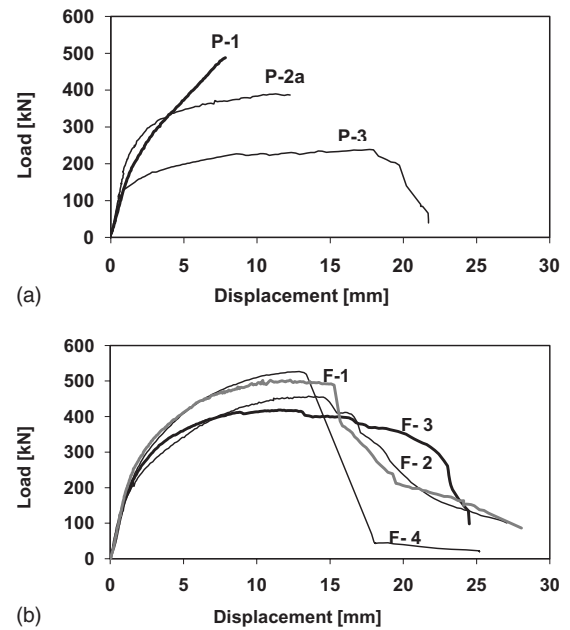| Specimen	Steel fiber % by volume	Compressive strength (Day of testing) (MPa)	Splitting tensile strength (MPa)	Fracture energy (J/m^2)
P-1[a]	0.0	65.4	—	—
P-2a	0.0	68.5	4.8	—
P-3	0.0	68.5	5.62	—
F-1	1.0	59.9	7.35	13,095
F-2	1.0	54.8	8.05	9,920
F-3	1.0	56.2	—	9,988
F-4	1.5	48.6	—	15,545

[a]=130 mm thickness; 127 mm for all others.

concrete compression strength. With all SFRC specimens, the loading plate penetrated approximately 15 mm at failure.

In general, as the transverse load increases and the slab flexes and cracks, an in-plane expansion of the slab will occur. If this expansion is restrained, increased axial compression forces will be induced thus giving rise to "membrane action" or "arching action." In the specimens tested, the lateral straining was passively resisted by the post-tensioning system; this resulted in an increase in force in the post-tensioning bars and hence in the prestress on the slabs. At ultimate load, the increase in in-plane axial force was as much as 50% or more (see Table 3), significantly influencing load capacity and behavior. The variation of the in-plane load corresponding to the applied vertical load is illus-

(a)

(b)

Fig. 2. Measured load-deformation responses: (a) plain concrete specimens; (b) FRC specimens

trated for all the specimens in Fig. 4; the in-plane axial forces began to diminish once the specimen entered the postpeak regime.

Discussion

Comparing the results for both the normal concrete (P-1, P-2a, P-3) and fiber concrete (F-1, F-2, F-3 and F-4) specimens, it is seen that the level of prestress influenced all aspects of behavior, including cracking, deflection, stiffness, and failure mode. The influences on ultimate load and absorbed energy are represented in Table 4. As one might expect, increasing the prestress level enhanced the ultimate load capacity and stiffness but had a negative effect on ductility. This conclusion is also clearly verified by the comparison of deformation and load capacities responses for Specimens P-1, P-2a and P-3 in Fig. 2(a). The increases in the ultimate load and stiffness can be attributed to the increased membrane action which, in turn, was affected by the level of the in-plane axial stress.

Comparing the behavior of Specimen P-1 to that of Specimen F-1, and of Specimen P-2a to that of Specimen F-3, for the same

Table 3. Prestressing Force/Stress (In-Plane Axial Force/Stress) of the Specimens

Specimen	P_{max} (kN)	N-S direction				E-W direction			
		Initial		at P_{max}		Initial		at P_{max}	
		load (kN)	stress (MPa)	load (kN)	stress (MPa)	load (kN)	stress (MPa)	load (kN)	stress (MPa)
P-1	488	1192	6.1	1508	7.7	1162	6.0	1282	6.6
P-2a	390	925	4.9	1257	6.6	790	4.1	967	5.1
P-3	239	417	2.2	1069	5.6	366	1.9	765	4.0
F-1	503	1148	6.0	1423	7.5	1135	6.0	1377	7.2
F-2	457	861	4.5	1230	6.5	1110	5.8	1231	6.5
F-3	419	779	4.1	971	5.1	780	4.1	839	4.4
F-4	527	1167	6.1	1443	7.6	962	5.0	1105	5.8

Table 4. Specimen Test Results

Specimen	Strength and failure mode				Strain energy absorbed			
	P_{max} (kN)	$\Delta_{P\,max}$ (mm)	Failure mode	Nature of failure	$U_{P\,max}$ (J)	U_{80} (J)	$U_{\Delta\,max}$ (J)	Ductility $[U_{\Delta\,max}/U_{P\,max}]$
P-1	488	7.84	Punching	Brittle	2419	—	2419	1.00
P-2a	390	11.28	Punching	Brittle	3625	—	4007	1.10
P-3	239	17.68	Punching-Flexural	Moderately ductile	3636	4078	4313	1.19
F-1	503	12.28	Punching	Moderately ductile	4836	6498	9004	1.86
F-2	457	14.02	Punching	Moderately ductile	4966	6251	8214	1.65
F-3	419	11.49	Punching	Moderately ductile	3843	7429	8383	2.18
F-4	527	12.89	Punching	Moderately brittle	5202	—	7018	1.35

P_{max}=Failure load; $\Delta_{P\,max}$=Displacement at the P_{max}; $U_{P\,max}$=Strain energy calculated up to peak load; U_{80}=Strain energy calculated up to 80% of the max load at the post-peak; $U_{\Delta\,max}$=Strain energy calculated up to the max displacement.

prestressing levels, adding steel fibers (V_f=1%) resulted in the transition from a brittle to a ductile punching shear failure, and improved the postcracking behavior and postpeak load-carrying capacity. The improvements in the strain energy absorption capacity can be attributed to the energy absorbed in debonding, stretching and pulling-out of the fibers after cracking. In addition, the presence of fibers prevented the propagation of the shear crack from the tension zone to the compression zone (top surface), impeding the formation of the failure cone observed in Specimens P-1 and P-2a; Specimens F-1 and F-3 remained intact after failure. However, the ultimate punching resistance (P_{max}) increased by only 10%. It is observed that fiber inclusion has less of a

beneficial effect on ultimate load when combined with in-plane axial restraint. [Swamy and Ali (1982) reported an increase of 40% in the ultimate resistance corresponding to 1% of fiber volume in unrestrained specimens.]. As for Specimen F-4, with 1.5% fiber, the test results indicate only a 5% increase in the ultimate punching resistance compared to that of Specimen F-1 (similar concrete strength and prestressing levels but 1% fiber). This may be due to significant bond deterioration of the steel fibers at the crack locations caused by the shear punching failure mechanism under high prestressing loads.

Varying the axial stresses in one direction had only a minor influence on the general behavior of the specimens tested. For Specimen F-1 and Specimen F-2, an inplane axial stress of approximately 6.0 MPa was applied in one direction, while the inplane axial stresses in the orthogonal direction were 6.0 MPa and 4.5 MPa, respectively. Both specimens experienced similar load-deformation behavior, strain energy absorption capability, and failure mode. The failure load for F-1 increased by only 5%, and the energy absorption capacity remained virtually unchanged.

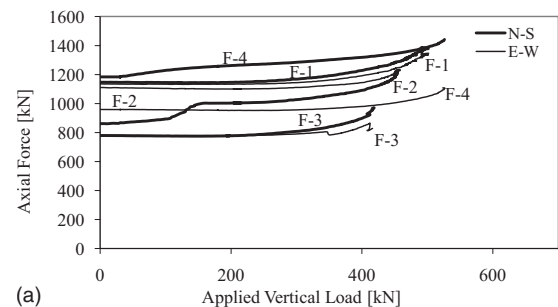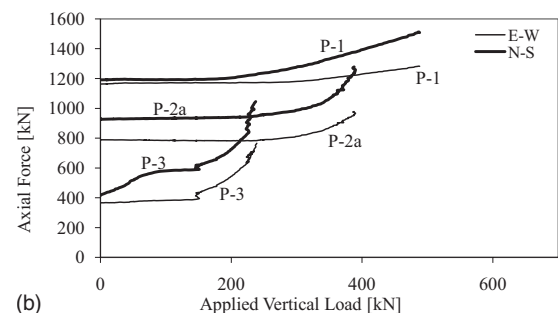In-plane axial force applied to the slabs can induce significant

(a)

(b)

Fig. 3. Test specimens at failure: (a) specimen P-1 lifted up after the test and debris of the specimen on the support set up; (b) Specimen F-2 (cracks on the tension face)
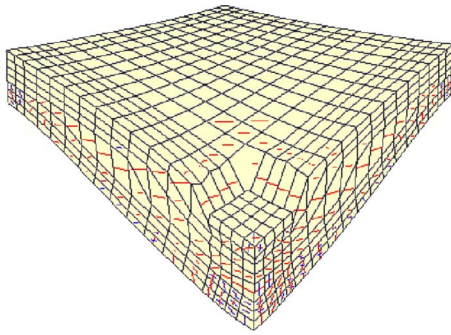

(a)

(b)

Fig. 4. Variation of in-plane axial load: (a) slabs with steel FRC; (b) slabs with plain concrete

Fig. 5. Mesh and cracks pattern P-1 obtained from FE analysis of specimen P-1 (using symmetry, one-quarter of the slab was modeled)

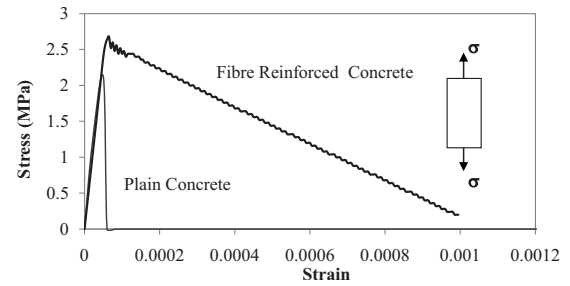**Fig. 6.** Comparison of tension stress-strain curves for steel FRC and plain concrete

moments at large deformations especially for ductile slab such those with fibers. Furthermore, in long-term, creep and shrinkage of the concrete could result in reduction of the in-plane axial force, which would influence the punching shear capacity of the post-tensioned slabs. Further studies are recommended to evaluate these effects.

Numerical Modeling

The specimens were modeled for nonlinear finite-element analysis (NLFEA) using program VecTor3. This program, developed specifically for the analysis of reinforced concrete solids, is based on the smeared rotating crack approach. RC is modeled as an isotropic material before cracking, and as an orthotropic material afterwards. The material models and constitutive relations used are based on the Disturbed Stress Field Model (DSFM) (Vecchio 2000), which is an extension of the Modified Compression Field Theory (MCFT) developed by Vecchio and Collins (1986). The program is based on an iterative total stress and strain formulation in which secant moduli are defined and progressively refined according to current local stress-strain states.

Due to symmetry, only one-quarter of the typical test specimen needed to be modeled. The FE mesh employed, shown in Fig. 5, consisted of 2,039 constant-strain hexahedron elements and 2,648 nodes. For better distribution of the imposed vertical load and to prevent local failure, the loading plate was also modeled. All nodes across the axes of symmetry were restrained against in-plane displacement. Nodes corresponding to the location of the roller supports (bottom layer at 75 mm from the edges) were restrained in the z-direction with "compression-only" vertical truss members, thus permitting "lift-off" in the modeling. Vertical loading was modeled as an imposed downward displacement at the node corresponding to center of the loading plate. Axial stresses were applied as concentrated loads in both orthogonal directions, distributed over nodes along the edges. These in-plane axial forces were increased in fixed proportion to the applied vertical displacement. The constant increase rate of in-plane axial force for each slab was determined based on the average increase rate of the prestressing force, corresponding to the vertical displacement, measured during the test.

To model the post-cracking tensile behavior of FRC, a cursory version of the Variable Engagement Model, developed by Foster et al. (2006), was used. As an example, an analysis was implemented using the Foster model to estimate tension stress-strain response of a SFRC element with material properties similar to that of the specimen F-1. Fig. 6 illustrates the results. For the sake

of comparison, the tension response of a plain concrete with identical compression strength is also plotted. Except for the tension modeling, all other material modeling was done using the default options of the program.

The load-deformation responses determined from the FE analyses are compared to the experimentally observed behaviors in Fig. 7. In general, the ultimate load capacity, pre- and post-cracking stiffness, ultimate ductility and energy absorption capacity were calculated with reasonable accuracy. In all cases, the failure modes were reasonably captured. The ratio of the experimental to calculated strengths had a mean of 1.01 and a coefficient of variation of 10% (see Table 5). Improved simulations might be expected once a more refined model for the post-cracking tensile stress response of SFRC can be developed and implemented into the FE formulation.

Codes and Analytical Model Predictions

ACI 318-99 (Clause 11.12.2.2) has been used to estimate the punching shear strength of prestressed slabs according to the following equation:

$$V_c = (0.083\beta_p \sqrt{f_c'} + 0.3f_{pc})b_o d + V_P \qquad (1)$$

Where, for the specimens in this study with square loaded areas, V_c=available shear strength; N, b_o=$(4b+\pi d)$, mm, d=effective slab depth (need not be taken less than 0.8t for prestressed concrete slabs, which is the case for all the test specimens), mm, t=slab thickness, mm, f_c'=concrete cylinder strength, MPa, β_p=3.5 (for all specimens), f_{pc}=average value of axial stress in the two directions, which shall not be less than 0.9 MPa or greater than 3.5 MPa, and V_P=vertical component of all effective prestress forces crossing the critical section which is zero for the slabs in this study.

Canadian standard CSA A23.3-04 (Clause 18.12.3.3) was also employed to determine the punching shear strength of the prestressed slabs, according to the following equation:

$$V_c = \left(\beta_p \phi_c \sqrt{f_c'} \sqrt{1 + \frac{\phi_p f_{cp}}{0.33\phi_c \sqrt{f_c'}}}\right)b_o d + V_p \qquad (2)$$

and where f_{cp}=average value of axial stress in the two directions not to exceed 3.5MPa, and b_o=perimeter of the critical section. Similar to the ACI equation, the second term in Eq. (2) represents the vertical component of the prestressing force, which is zero for all the specimens considered here. For the analysis, the resistance factor for concrete, ϕ_c and ϕ_p were taken as unity, β_p as 0.33, and d as 0.80t. Table 6 summarizes the strength of the test slabs, determined accordingly.
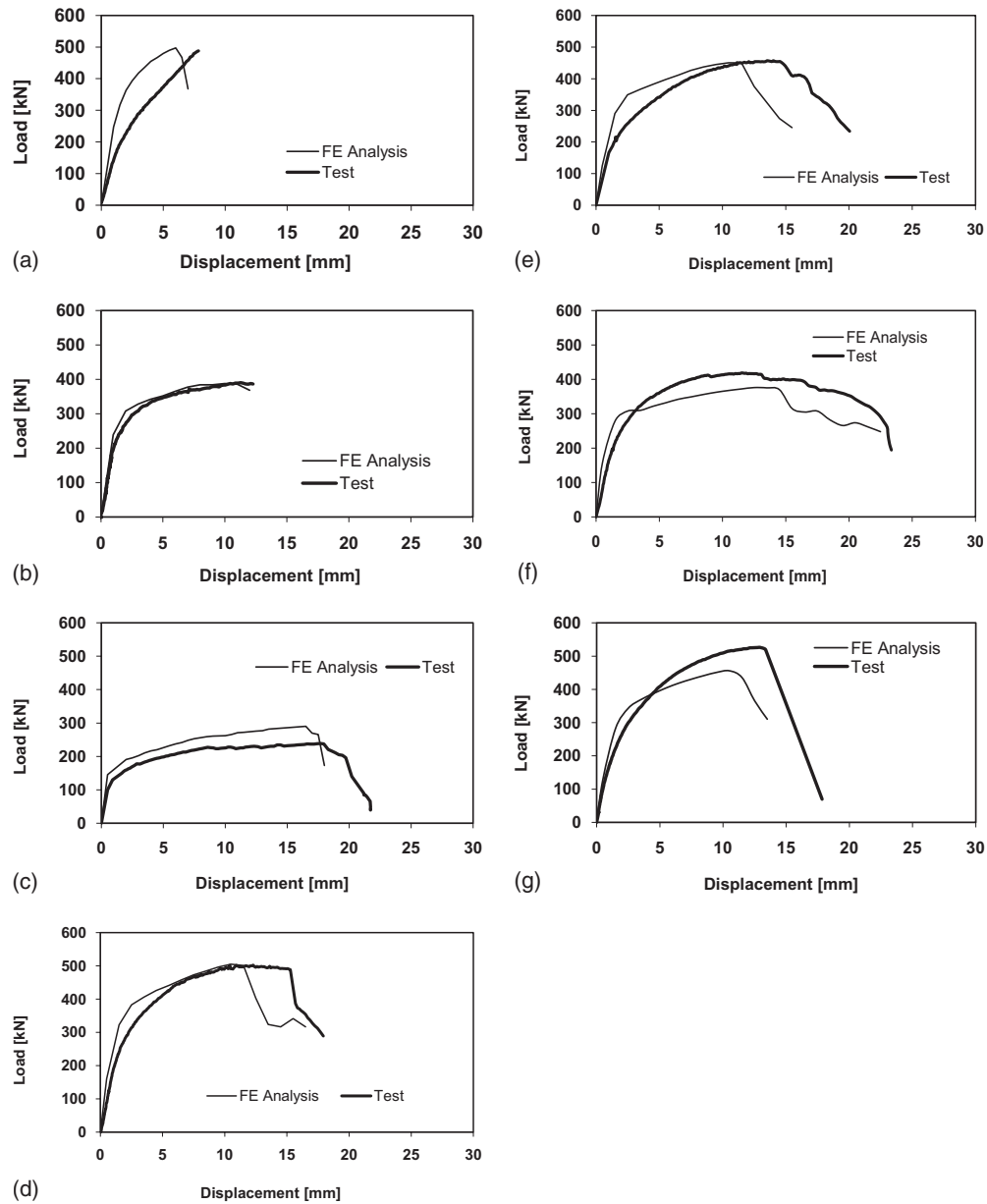
Fig. 7. Comparison of calculated and experimental load-deformation responses of the different specimens: (a) P-1; (b) P-2a; (c) P-3; (d) F-1; (e) F-2; (f) F-3; and (g) F-4

It is important to note that the design values for f_{pc}/f_{cp} in the ACI and CSA codes are limited due to lack of test data for higher values. Further, f_c', the concrete strength in both codes, cannot exceed 35 MPa. The main purpose of employing the ACI and CSA equations in this study is to evaluate their applicability for the specimens tested with higher concrete strength and higher in-plane axial stress. Therefore, these two limits have not been considered in the calculation; the exact values of concrete compression strength and in-plane axial stress have been employed in Eqs. (1) and (2).

Comparison reveals that more reasonable estimations were achieved using the ACI code equation than with the CSA code equation. The CSA equation overestimated the shear capacity for all the specimens except F-4 by about 20%. Both equations predicted the punching shear capacity with relatively more accuracy for Specimens P-1 and, surprisingly, Specimens F-1–3. However, the code equations did not make any allowance for the beneficial

Table 5. FE Analysis Results

Specimen	Max. load, $P_{theor.}$ (kN)	Disp. at P_{theor}, D_{theor} (mm)	$P_{exp.}/P_{theor.}$	$D_{exp.}/D_{theor.}$
P-1	497.0	6.0	0.98	1.31
P-2a	389.9	11.0	1.00	1.03
P-3	290.0	16.5	0.82	1.07
F-1	502.0	12.0	1.00	1.25
F-2	451.0	11.9	1.01	1.25
F-3	376.0	14.6	1.11	0.99
F-4	457.0	11.5	1.15	1.12
		Mean	1.01	1.15
		COV	10%	10%

Table 6. Punching Strengths Calculated Using ACI 318-99 and CSA A23.3

Specimen	$f_{average}$ (MPa)	d (mm)	b_o (mm) ACI	b_o (mm) CSA	$P_{calc.}$ (kN) ACI	$P_{calc.}$ (kN) CSA	$P_{exp.}$ (kN)	$P_{exp.}/P_{calc.}$ ACI	$P_{exp.}/P_{calc.}$ CSA
P-1	6.04	104.0	1127	1216	488	610	488	1.00	0.80
P-2a	4.49	101.6	1119	1206	427	545	390	0.91	0.72
P-3	2.06	101.6	1119	1206	343	443	239	0.70	0.54
F-1	6.00	101.6	1119	1206	460	573	503	1.09	0.88
F-2	5.17	101.6	1119	1206	420	528	457	1.09	0.87
F-3	4.09	101.6	1119	1206	387	494	419	1.08	0.85
F-4	5.55	101.6	1119	1206	420	521	527	1.26	1.01
							Mean	1.02	0.81
							COV	16%	17%

influence of the fibers. For Specimen P-2a, the ACI equation also overestimated the punching failure load. The failure mode of Specimen P-3 was combined flexural-punching and both ACI and CSA equations understandably overestimated the load capacity. Overall, the ratio of experimental to calculated strengths had a mean of 1.02 and a coefficient of variation of 16% for the ACI formulation, and a mean of 0.81 and a coefficient of variation of 17% for the CSA formulation. Table 6 summarizes the results of shear capacity calculations using both the ACI and CSA equations.

The model proposed by Hewitt and Batchelor (1975) was also used to predict the punching shear capacity of the test specimens. This model is based on idealization of the slab as a circular slab that fails in punching, considering the fractured slab at failure. The main geometrical and material parameters considered in the analysis are: depth of the concrete slab, diameter or equivalent diameter of the slab, diameter or equivalent diameter of the loading area, reinforcement ratio, yield stress of the steel, and the compressive strength of the concrete. This model presumes an axisymmetric slab configuration and loading condition. Thus, for calculation purposes, the equivalent diameter of the loaded area was taken as the diameter of the circle with the same perimeter as the square loading plate (255 mm), and the equivalent diameter of the slab was taken as the diameter of the largest circle which can be inscribed within the area of the slab (1,350 mm). The resulting predicted strengths are given in Table 7. The ratio of the experimental to calculated strengths had a mean of 1.11 and a coefficient of variation of 12%. It was found that the Hewitt and Batchelor model provided slightly conservative estimates of strength in all cases expect specimen P-1.

Table 7. Punching Strengths Calculated Using Hewitt and Batchelor Model

Specimen	$F_{average}$ (kN)	F1[a] (kN/m)	$P_{theor.}$ (kN)	$\Delta_{theor.}$ (mm)	$P_{exp.}/P_{calc.}$
P-1	1177	784.7	521	4.12	0.94
P-2a	857	571.3	381	5.3	1.02
P-3	391	260.7	175	10.17	1.37
F-1	1141	760.7	491	4	1.02
F-2	985	656.7	428	4	1.07
F-3	779	519.3	346	5.2	1.21
F-4	1064	709.3	455	4	1.16
				Mean	1.11
				COV	12%

[a]=Average axial force per unit length ($F_{average}/1.5$).

Conclusions

A series of externally post-tensioned concrete slabs, comprising specimens constructed of normal and FRC, was subjected to punching shear loads in a specially devised testing rig. The test results, coupled with results of analytical and numerical investigations, suggested the following conclusions:

1. In-plane axial compressive stress, derived from external post-tensioning of the slabs, resulted in significant increases in punching shear load capacity.
2. Inclusion of fiber in the concrete also resulted in significant improvements in behavior, particularly with respect to ductility, energy dissipation, and non-brittleness of failure.
3. Varying the prestressing in one direction, relative to the perpendicular direction, did not have a significant influence on behavior (as deduced by comparing Specimens F-1 and F-2).
4. Reasonably accurate correlations were obtained between the nonlinear FE analysis results and the test results.
5. While the ACI code equation provided reasonably accurate estimates for punching shear capacities of the specimens as a whole, it tended to oversestimate the strengths of the plain concrete specimens and underestimate the strengths of the FRC specimens.
6. The CSA A23.3 code relationship for punching strength of slabs gave generally unconservative estimates of the load capacity of the test slabs.
7. The Hewitt and Batchelor model gave generally slightly conservative estimates of the load capacity of the test slabs.

The results of the experimental investigation support the premise that use of post-tensioned, fiber-reinforced concrete is a viable option in optimizing the design of deck structures in high-performance concrete bridges.

Notation

The following symbols are used in this paper:

b_o = shear perimeter defined differently in different code, mm;

d = effective slab depth, for all specimens, $d=0.8t$, mm;

f'_c = concrete cylinder strength, Mpa;

f_{cp} = in-plane axial stress, prestressing, in each direction, for CSA code equations, MPa;

f_{pc} = in-plane axial stress, prestressing, in each direction, for ACI code equations, MPa;

t = total slab thickness, mm;

V_c = available punching shear strength, N;

V_P = vertical component of all effective prestress forces crossing the critical section which is zero for all the slabs in this study, N;

β_p = in the ACI equation, it is 3.5 and in the CSA equation, it is 0.33 for all the specimens;

ϕ_c = resistance factor for concrete=1.0 for analysis; and

ϕ_p = resistance factor for prestressing tendons=1.0 for analysis.

References

Aoki, Y., and Seki, H. (1974). "Shearing strength and cracking in two-way slabs subjected to concentrated load." Cracking, Deflection, and Ultimate Load of Concrete Slab Systems. *J. Am. Concr. Inst.*, 30, 103–126.

Foster, S. J., Voo, Y. L., and Chong, K. T. (2006). "FE Analysis of steel fibre reinforced concrete beams failing in shear: Variable engagement model." *ACI SP-237 Finite element analysis of reinforced concrete structures*.

Hassan, A., Kawakami, M., Niitani, K., and Yoshioka, T. (2002). "Experimental investigation of steel-free deck slabs." *Can. J. Civ. Eng.*, 29(6), 831–841.

He, W. (1992). "Punching behaviour of composite bridge decks with transverse prestressing." Ph.D. thesis, Queen's Univ., Canada.

Hewitt, Brian E., and Batchelor, Barrington de V. (1975). "Punching shear strength of restrained slabs." *J. Struct. Div.*, 101(9), 1837–1853.

Kinnunen, S., and Nylander, H. (1960). "Punching of concrete slabs without shear reinforcement." *Transaction of the Royal Institute of Technology*, Stockholm, Sweden, 158.

Mufti, A. A., Jaeger, L. G., Bakht, B., and Wagner, L. D. (1993). "Experimental investigation of fibre-reinforced concrete deck slabs without internal steel reinforcement." *Can. J. Civ. Eng.*, 20(3), 398–406.

Newhook, J. P. (1997). "Behaviour of steel-free concrete bridge deck slabs under static loading conditions." Ph.D. thesis, Dalhousie Univ., Canada.

Shaaban, A. M., and Gesund, H. (1994). "Punching shear strength of steel fibre reinforced concrete flat plates." *ACI Struct. J.*, 91(4), 406–416.

Swamy, R. N., and Ali, S. A. R. (1982). "Punching shear behaviour of reinforced slab-column connections made with steel fibre concrete." *ACI J.*, 79(5), 392–406.

Taylor, R., and Hayes, B. (1965). "Some tests on the effect of edge restraint on punching shear in reinforced concrete slabs." *Mag. Concrete Res.*, 17(50), 39–44.

UNI-11039 (2003). *Steel fibre reinforced concrete. Part I: Definitions, classification specification and conformity. Part II: Test method for measuring first crack strength and ductility indexes*, UNI-Italian Organization for Standardization.

Vecchio, F. J. (2000). "Disturbed stress field model for reinforced concrete: Formulation." *J. Struct. Eng.*, 126(9), 1070–1077.

Vecchio, F. J., and Collins, M. P. (1986). "Modified compression field theory for reinforced concrete elements subjected to shear." *J. Am. Concr. Inst.*, 83(2), 219–231.

Wood, R. H. (1961). *Plastic and elastic design of slabs and plates*, Thames and Hudson, London, 253.